PLASMONIC PARTICLE ARRAYS ON LARGE AREAS FOR PHOTON MANAGEMENT

S. Jüchter[1], S.-K. Meisenheimer[1], H. Hauser[1], Ch. Wellens[1], O. Höhn[1], V. Kübler[1], T. Fix[1,2], U.T. Schwarz[3], B. Bläsi[1]

[1] Fraunhofer Institute for Solar Energy Systems ISE, Heidenhofstr. 2, 79110 Freiburg, Germany
Phone: +49 (0)761/4588-5967, Fax: +49 (0)761/4588-9981, E-Mail: sabrina.juechter@ise.fraunhofer.de
[2] ICube laboratory (Université de Strasbourg and CNRS), 23 Rue du Loess BP20 CR, 67037 Strasbourg Cedex 2, France
[3] Fraunhofer Institute for Applied Solid State Physics IAF, Tullastr. 72, 79108 Freiburg, Germany

ABSTRACT: In photovoltaic research, two major optimization directions have emerged: the realization of thinner cells while simultaneously reaching higher efficiencies. Therefore, photon management approaches become more and more important. A promising light trapping approach is the use of metallic nanoparticles revealing plasmonic effects. In plasmonics advantage is taken of scattering and the field enhancement around the nanostructure. This leads to an enhancement of the path lengths of light inside the solar cell, resulting in an enhanced absorption probability.
We present a fabrication process, applicable to large areas, to realize arrays of uniform, defined metallic nanoparticles using interference lithography, nanoimprint lithography and a lift-off process. The obtained nanoparticles are characterized with Fourier spectrometer measurements. The experimental results are then compared to Mie and rigorous coupled wave analysis simulations.

Keywords: Plasmonic, Nanoparticles, Light Trapping, Nanoimprint Lithography, Fabrication

1 INTRODUCTION

A major task in photovoltaics is the reduction of electricity production cost. To achieve this goal, two main trends have developed over the last decades. Firstly, there is an evolution towards thinner cells for a reduction of material costs. Secondly, steadily increased efficiencies are reached whereby a better ratio between overall system costs per watt is achieved. If the cell thickness is reduced, the diminished absorption of incoming light can cause a decrease of conversion efficiency. Consequently, the second optimization criterion of higher efficiencies cannot be reached anymore, implying an optimization trade-off. To solve this conflict, photon management structures become more and more important. Micron scale front side textures, e.g. random pyramids, are used for photon management in conventional silicon solar cells [1]. In high efficiency solar cells, more complex front side textures are used, e.g. inverted pyramids for monocrystalline silicon (c-Si) [1] or honeycomb textures on multicrystalline silicon (mc-Si) [2]. Textures on the micron scale are not applicable to thin or ultra-thin solar cells. A novel promising approach for photon management in such solar cells is the use of plasmonic resonances on metallic nanostructures [3].

In plasmonics two types of plasmons can be distinguished [3]: surface plasmon polaritons (SPP) supported by metallic surfaces and localized surface plasmons (LSP) on metallic nanoparticles. For SPPs, the incoming light is transformed into electron resonances traveling along a metal-dielectric interface. The LSP is the quantum of plasma oscillations of the free electron gas on a metallic particle.

In plasmonic photon management, the scattering and diffraction (Fig. 1a) of metallic particles can be used. The scattering of metallic nanoparticles is spectrally selective and can be tuned by changing the size of the particles, which is an important advantage for the use in solar cells. Additionally, directional scattering of incident light is possible because the particles scatter preferably into the dielectric with higher permittivity [4]. In combination with multiple scattering processes, scattering leads to a path length enhancement inside the solar cell. Furthermore, a strong field enhancement in the vicinity of the particle can be advantageous. By strong field enhancement around nanoparticles, the generation rate of electron-hole pairs can be improved or nonlinear processes can be supported, e.g. upconversion [5] (Fig. 1b)).
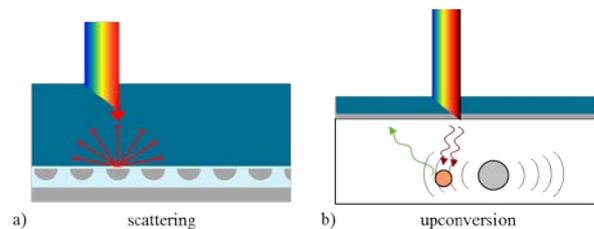

Figure 1: Sketches of two possible applications of plasmonic nanoparticles in solar cells by a) improving light trapping by scattering of incident light at the back or b) using the field enhancement around the particle to improve nonlinear processes such as upconversion.

The plasmonic scattering effect strongly depends on particle size and the surrounding material and has to be carefully tuned for the special application. The interesting size range of plasmonic nanoparticles as scattering centers in solar cells is around 100 nm [3], [6]-[10].

There are different approaches to fabricate plasmonic nanostructures [3]. In literature, predominantly results from self-organized metal particles can be found. These irregular structures with particles of varying dimensions show resonances for different wavelengths and also suffer from parasitic absorption as a result of this size distribution [11],[12]. This unwanted effect can be minimized by the fabrication of particles with uniform size distribution. Here, lithography techniques can be used, e.g. e-beam lithography. But in most cases these techniques have low throughput, are restricted to small areas and are expensive.

In this paper, a fabrication process for defined, ordered plasmonic nanoparticles applicable to large areas is presented. In section 2 the fabrication process based on interference lithography, nanoimprint lithography and lift-off is introduced. Firstly, the crossed grating master fabrication with interference lithography is described. Followed by the structure replication with nanoimprint

lithography and the optimization of the fabrication process starting with interference lithography are presented. In section 3 the optical properties of realized nanoparticles are compared to simulations with Mie theory and rigorous coupled wave analysis.

2 PREPARATION OF REGULAR PLASMONIC NANOPARTICLES

In order to use metallic nanostructures in solar cells, the challenge is to establish a large area applicable, cheap and high throughput fabrication process. The here investigated process chain starts with master structure production by interference lithography [13], followed by nanoimprint lithography, metallization and a lift-off step (schematically shown in Fig. 3) [14]. In the following the interference lithography master fabrication (section 2.1) and the replication process (section 2.2) ending up in metallic nanoparticles are explained separately.

2.1 Interference lithography for master fabrication

In Fig. 2, the interference lithography setup for crossed grating master fabrication is shown schematically. A laser is used as the light source for interference lithography. The laser beam is split into two beams that are expanded and superimposed on a photoresist coated sample. The resulting interference pattern is used to expose the photoresist, in analogy to classical photo lithography. In this way, a multiplicity of surface structures can be generated on large areas. A single exposure as sketched in Fig. 2 results in a line grating. For the here used crossed grating two exposures have to be done on the same sample. Rotating the sample after first exposure opens up the possibility to generate crossed or hexagonal gratings.
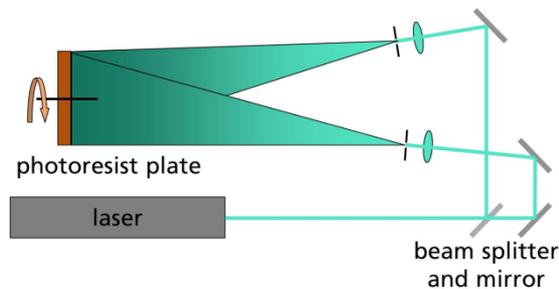

Figure 2: Schematic view of crossed grating master structure fabrication with an interference lithography process. A two wave interference lithography setup is used to expose a photoresist coated sample twice to generate a crossed grating. A single exposure using this setup leads to a line grating. The orange arrow indicates a rotation of the sample after the first exposure. After sample rotation by 90°, the second exposure results in a crossed grating. The strength of interference lithography is that nanostructures on areas up to 1.2 x 1.2 m² [13] can be originated.

2.2 Structure replication by nanoimprint lithography

For replication of the master structure, nanoimprint lithography is used. In this process, a flexible stamp is molded and pressed into a resist coated on a sample (Fig. 3 b). After imprinting a reactive ion etching (RIE) step is carried out to remove the residual resist layer (Fig. 3 c).
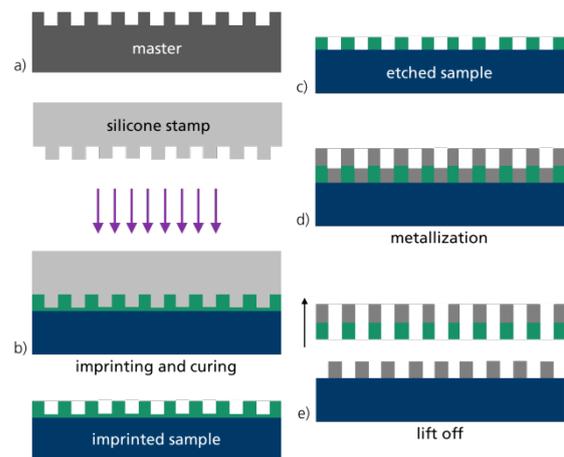

Figure 3: Sketch of the fabrication of metallic nanoparticles using nanoimprint lithography. From the master structure, generated by interference lithography, a silicone stamp is molded (a). This stamp is pressed into a resist, which is cross-linked using UV light (b). The patterned resist is etched in a reactive ion etching (RIE) process after demolding the stamp (c). Afterwards the substrate is metallized (d) and the last step is a lift-off (e).

The photoresist master structure from interference lithography is replicated in a first step in nickel by electroplating. This nickel master is used as the starting point for nanoimprint lithography. In the next step, from the nickel master the flexible stamp is molded (Fig. 4 a). For this replication, silicone is used. Using silicone, it is not possible to replicate arbitrarily small features because of the limited modulus of elasticity. Therefore, silicone stacks with adapted shore hardness are used, as demonstrated in [15]. In this way, structure fidelity in combination with good surface adaptability is reached. A two layer configuration with a soft silicone block for surface adaptability and a hard silicone layer for accurate pattern replication is molded.
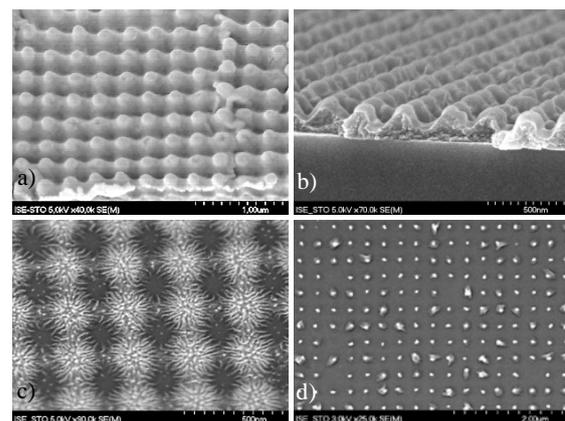

Figure 4: Scanning electron microscopy images of the silicone stamp (a), a sample after imprinting (b) and etching (c) and a successful lift-off of the resist after silver deposition using sputtering (d). The resulting silver nanoparticles have a period of 300 nm and a diameter of approx. 70 nm.

The silicone stamp is then used for the actual replication process via nanoimprint lithography. Therefor, the stamp is pressed into a UV-curable resist that has been spin coated on a substrate before (Fig. 4 b). Between the glass substrate and the imprint resist, an

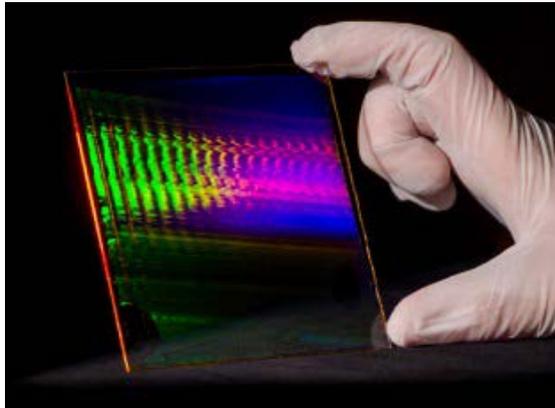adhesion promoter is used which serves later on as sacrificial layer for the lift-off.

Figure 5: Picture of a patterned photo resist on a 100 x 100 mm² glass substrate structured by nanoimprint lithography (Fig. 3 b).

After the cross-linking of the resist, the stamp is demolded and can be used for further imprints. A picture of such an imprint is shown in Fig. 5. Prior to metallization a RIE step is carried out to open up the imprint structure down to the substrate (Fig. 4 c) to prevent the lift-off of the particles. Finally, the patterned resist is metallized and the lift-off supported by the sacrificial layer is carried out. For metallization, sputtering or evaporation can be used. Fig. 4 d) shows, the obtained metallic nanoparticles. The particles with a diameter of approx. 70 nm are arranged in a crossed grating with 300 nm period on a glass substrate with total area of 100 x 100 mm².
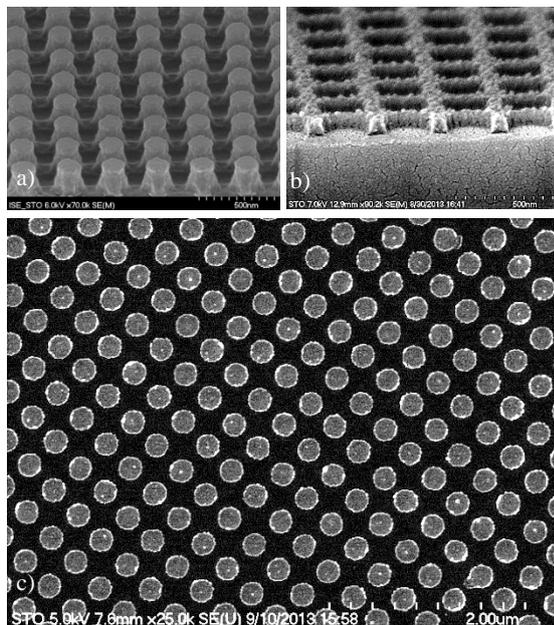

Figure 6: Scanning electron microscopy images of the improved interference lithography master structure in photo resist (a), a sample after imprinting and etching (b) and a successful lift-off of the resist after silver deposition using sputtering (c). The resulting silver nanoparticles have a period of 300 nm and a diameter of approx. 200 nm.

In particle processing the rounded shape of the master structure is adverse. The resulting sinusoidal shape of the imprinted resist (see Fig. 4 b) affects the fabrication of metallic nanoparticles negatively. Furthermore, the RIE process step strongly attacks the imprinted resist (see Fig. 4 c), resulting in grooves on the surface, which deteriorates the particle fabrication in addition.

To solve the problem of rounded faces after imprinting a new interference lithography master structure with steep faces was realized (Fig. 6 a). This steeper structure creates an improved starting point for the replication process with nanoimprint lithography. Besides this, a changed etching process leads to less resist damage (Fig. 6 b).

Through the new process management, steeper faces and lower resist damage could be realized. With the new process uniform Ag nanoparticles arranged in a crossed grating with 300 nm period and particle diameter of approx. 200 nm could be obtained. In Fig. 6 c) the realized particles are shown.

3 OPTICAL CHARACTERIZATION AND COMPARISON TO SIMULATION

The obtained 70 nm diameter metallic nanoparticles on a glass substrate were in a first step embedded into a medium with refractive index of 1.475, very close to the refractive index of glass. The embedding is necessary to protect the Ag particles from degradation. Furthermore, in solar cell application the particles would also be embedded, e.g. in SiO_2 or SiN. The samples are characterized optically by Fourier spectrometer measurements. Here, the reflectance R and transmittance T of the sample were measured with the help of an integrating sphere. In a first step a hemispherical reflectance and transmittance measurement is made. All light which is scattered or transmitted by the sample is collected, including the direct part of the measuring beam. Using

$$A = 1 - R - T, \qquad (1)$$

the absorptance A is calculated from the reflectance (R) and transmittance (T) data.

In Fig. 7, the absorptance corrected by the glass reference is plotted against wavelength for the investigated Ag nanoparticles on a glass substrate embedded into a medium with refractive index of 1.475.

An absorption increase with a maximum at 460 nm can be observed. It could be assumed, that the increase in absorption is caused by an increase in absorption in the Ag. Considering a simplified description of the experimentally realized configuration, Mie calculations of an Ag sphere embedded in a medium can be performed. For this calculation, a Mathematica code written by A. Lompado [16] was used. In Fig. 7, the simulation result of an Ag sphere with radius of 35 nm embedded in glass is shown in red.
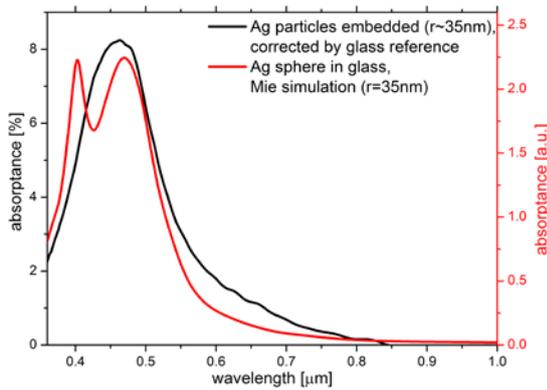
Figure 7: Optical characterization of embedded nanoparticles in comparison to a Mie simulation. Shown is the absorptance A of silver nanoparticles (300 nm period, approx. 70 nm diameter) embedded into a medium of n=1.475 on a glass substrate (black) corrected by glass reference using a Fourier spectrometer. Measured were reflectance (R) and transmittance (T) in hemispherical configuration with an integrating sphere. From reflection and transmission data the absorption was calculated using (1). In red, the Mie simulation [16] for an Ag sphere in glass with 70 nm diameter is shown.

A comparison of the experimental and simulated data, shows the same peak position at approx. 460 nm. From this, it can be concluded that the simplified description by Mie theory is useful to analyze the experimentally fabricated particles.

To estimate the positive effect of metallic nanoparticles in solar cells the scattering behavior of the particles is of particular interest. Therefore in a second step, the embedded Ag nanoparticles were additionally investigated by a Fourier spectrometer measurement capturing the diffuse part in reflection and transmission. In contrast to the hemispherical measurement, here only the part of incoming light scattered by the sample is measured as the direct part of the beam can exit the integrating sphere. Normalizing the diffuse value by the hemispherical value, the fraction of scattered light in reflection or transmission can be calculated:

$$\text{fraction of scattered light} = \frac{\text{diffuse}}{\text{hemispherical}}. \qquad (2)$$

In Fig. 8, the calculated fraction of scattered light in reflection and transmission is plotted against wavelength.

For the scattered fraction of reflected light, a peak can be seen in. Furthermore, the fraction of scattered light is higher in reflection than in transmission. This attribute is especially relevant for light trapping at the back of a solar cell because it is of great importance to scatter light transmitted by the solar cell back into the silicon. Furthermore, this maintain the already mentioned possibility of directional scattering. The higher fraction of scattered light in reflection, in combination with a high refractive index substrate material as in silicon solar cells, can lead to a good light trapping effect because the scattering is preferably directed into the solar cell.
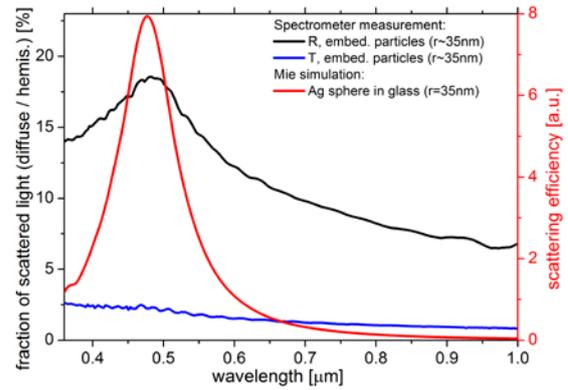

Figure 8: Optical characterizations of silver nanoparticles (300 nm period, approx. 70 nm diameter) embedded into a medium of n=1.475 on a glass substrate using a Fourier spectrometer. Measured were reflectance (R) and transmittance (T) in diffuse and hemispherical configuration with an integrating sphere. Shown is the fraction of scattered light (diffuse measurement normalized by hemispherical data using (2), left axis) of an embedded sample. For comparison with Mie theory, calculated scattering efficiency [16] for an Ag sphere embedded in glass with a diameter of 70 nm is plotted in red (right axis).

In Fig. 8 the scattering efficiency calculated by Mie theory [16] of an Ag nanoparticle with 35 nm radius in glass is plotted in red. A comparison of the experimental (black) with the calculated scattering efficiency shows a scattering peak at the same position. The simplified description by Mie theory as useful method to analyze the experimentally fabricated particles was again confirmed.

In the experiment the Ag particles are realized on a glass substrate. This means at the interface between the glass substrate and the surrounding air. These samples were also investigated by hemispherical Fourier spectrometer measurements in reflection and transmission. Fig. 9 shows the calculated absorptance (black) using equation (1) of Ag nanoparticles (300 nm period, approx. 70 nm diameter) on a glass substrate, where the medium on the Ag side is air. An absorption enhancement with a peak at 420 nm can be seen.

This experimentally realized configuration cannot be described by Mie theory anymore. In Mie the assumption is made, that only one particle completely embedded in a medium is considered. Therefore, for comparison between experiment and simulation a method is needed in which an array of particles at an interface can be implemented. Hence, the Rigorous Coupled Wave Analysis (RCWA) [17],[18] written in MATLAB by Philippe Lalanne and Jean-Paul Hugonin [19] is used. The simulated absorptance is plotted in red in Fig. 9.
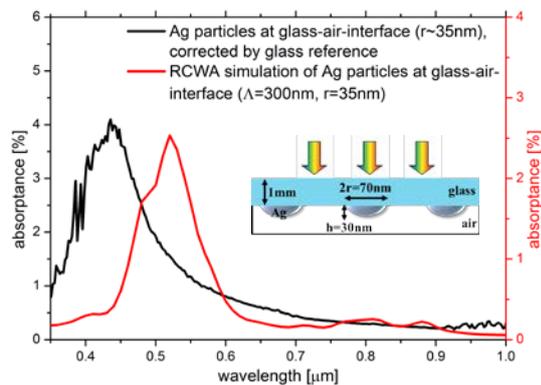
Figure 9: Optical characterization of silver nanoparticles (300 nm period, approx. 70 nm diameter) on glass substrate in air using a Fourier spectrometer. Measured were reflectance (R) and transmittance (T) in hemispherical configuration with an integrating sphere. Shown is the calculated absorptance (black) using (1). For comparison, results of RCWA simulations [17]-[19] of Ag nanoparticles arranged in a crossed grating with 300 nm period and 35 nm radius at a glass-air-interface are shown in red. The inset displays the experimental as well as the simulation configuration.

The geometry of the simulated particles in RCWA is an approximation of the obtained particles. The particle representation in simulation cannot match directly the experimentally realized particles. The simulation shows an absorption enhancement with peak at approx. 520 nm. This simulation peak is red-shifted compared to experiment. Differences in particle features or refractive indices could be responsible for such a shift. The refractive indices implemented in the simulations do not necessarily describe the materials used in the experiment adequately. Identifying the refractive indices of noble metals like silver is particularly difficult [20].

Besides the far field analysis, with RCWA also the near field around the particles can be investigated. In Fig. 10 a cross section through the center of an Ag particle arranged in a crossed grating with 300 nm period and 150 nm diameter on 10 µm silicon is shown. The field intensity is plotted against position for the resonance wavelength of this simulation configuration.
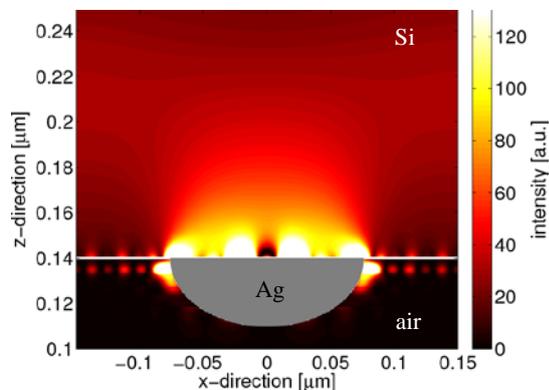

Figure 10: Near field simulation of an Ag nanoparticle (crossed grating, 300 nm period, 150 nm diameter, 30 nm high) at a silicon (10 µm)-air-interface using RCWA [17]-[19]. Shown is a cross section through the center of the Ag nanoparticle at resonance wavelength (1300 nm).

It can be seen that in the vicinity of the particle the field intensity in the silicon increases drastically. This near field enhancement around the particle can be used to improve e.g. nonlinear processes like upconversion as mentioned before.

4 CONCLUSIONS

Periodically arranged silver nanoparticles fabricated by a process based on interference lithography, nanoimprint lithography and a lift-off is presented. With this process chain, Ag nanoparticles arranged in a crossed grating with 300 nm period and approx. 70 nm and 200 nm diameter were fabricated on glass substrates. Particle substrates with 70 nm diameter were investigated using Fourier spectrometer measurements. Initially, an absorption enhancement could be demonstrated for embedded particles and a higher fraction of scattered light in reflection was measured. The obtained measurement results for embedded particles show good accordance with Mie simulations. Comparing RCWA simulations with measurements of Ag particles fabricated on a glass substrate show different absorption peak positions. This shift could be attributed to the difference of refractive indices in simulated and experimentally realized materials, because identifying the refractive indices of noble metals like silver in experiments is particularly difficult [20]. The presented results are overall promising. The investigated process chain allows the fabrication of periodically arranged metallic nanoparticles for the use in solar cells. The measured scattering peak is at shorter wavelength than necessary for enhancing the efficiency of thin silicon solar cells. This was expected since glass was used as substrate material, which has a lower refractive index than silicon. The next step is the fabrication and investigation of these Ag nanostructures on silicon, which is at the moment ongoing work.

As a future perspective, the presented fabrication process can be extended to larger areas by replacing the simple imprinting step by a roller-nanoimprint lithography (roller-NIL) [21] process. The roller-NIL process allows an in-line replication on full wafers and with this the integration into the solar cell production process.

5 ACKNOWLEDGMENT

6 REFERENCES

[1] P. Campbell and M.A. Green, J. Appl. Phys., 62(1), 243-249 (1987).

[2] O. Schultz, S.W. Glunz and G.P. Willeke, Prog. Photovolt: Res. Appl., 12, 553–558 (2004).

[3] H.A. Atwater and A. Polman, Nature Materials, 9, 205-213 (2010).

[4] J. Mertz, J. Opt. Soc. Am. B, 17, 1906-1913 (2000).

[5] F. Auzel, Chem. Rev., 104, 139-174 (2004).

[6] K.R. Catchpole and A. Polman, Appl. Phys. Lett., 93, 191113 (2008).

[7] V.E. Ferry, M.A. Verschuuren, H.B.T. Li, E. Verhagen, R.J. Walters, R.E.I. Schropp, H.A. Atwater and A. Polman, Opt. Express, 18, A237-A245 (2010).

[8] F.J. Beck, E. Verhagen, S. Mokkapati, A. Polman and K.R. Catchpole, Opt. Express, 19, A146-A156 (2011).

[9] S. Pillai, F.J. Beck, K.R. Catchpole, Z. Ouyang and M.A. Green, J. Appl. Phys., 109, 073105 (2011).

[10] U.W. Paetzold, E. Moulin, B.E. Pieters, R. Carius and U. Rau, Opt. Express, 19, A1219-A1230 (2011).

[11] Z. Ouyang, X. Zhao, S. Varlamov, Y. Tao, J. Wong and S. Pillai, Prog. Photovoltaics Res. Appl., 1-11 (2011).

[12] E.-C. Wang, S. Mokkapati, T. Soderstrom, S. Varlamov and K. Catchpole, IEEE Journal of Photovoltaics, *3*, 267-270 (2013).

[13] A.J. Wolf, H. Hauser, V. Kübler, Ch. Walk, O. Höhn and B. Bläsi, Microelectronic Engineering, 98, 293 - 296 (2012).

[14] S. Jüchter, H. Hauser, C. Wellens, M. Peters, J.-C. Goldschmidt, U. Schwarz, and B. Bläsi, Proc. SPIE 8438 (2012)

[15] H. Schmid and B. Michel, Macromolecules, 33, 3042-3049 (2000).

[16] A. Lompado, Mie Mathematica Code (2002), http://www.scattport.org/index.php/programs-menu/mie-type-codes-menu/112-mie-mathematica-lampado

[17] M.G. Moharam and T.K. Gaylord, J. Opt. Soc. Am., 72, 1385-1392 (1982).

[18] M.G. Moharam and T.K. Gaylord, J. Opt. Soc. Am. A, 3, 1780–1787 (1986).

[19] Ph. Lalanne and M.P. Jurek, J. Mod. Optics, 45, 1357-1374 (1998).

[20] M.A. Green and S. Pillai, Nature Photonics, 6, 130-132 (2012).

[21] H. Hauser, B. Michl, S. Schwarzkopf, V. Kübler, C. Müller, M. Hermle and B. Bläsi, IEEE J. Photovoltaics, doi:10.1109/JPHOTOV.2012.2184265.